Emerging Shift in the Indian Summer Monsoon Sensitivity to Equatorial Indian Ocean Sea Surface Temperature Anomalies: Insights from High-Resolution AGCM SST Patch Experiments

K. H. Usha[1,2,*], Sajani Surendran[1,2], Kavirajan Rajendran[1,2,3], Hirokazu Endo[4] and Akio Kitoh[4]

[1]CSIR Fourth Paradigm Institute, Bengaluru, India.

[2]Academy of Scientific and Innovative Research (AcSIR), Ghaziabad 201002, India

[3]Institute for Climate Change Studies, Kottayam, India.

[4]Meteorological Research Institute, Tsukuba, Japan.

[*]Corresponding author: Usha K H (usha.4pi@csir.res.in)

Key Words:

- Indian Summer Monsoon
- Equatorial Indo-Pacific Climate Modes
- Sea Surface Temperature Anomalies
- Western Equatorial Indian Ocean (WEIO) Warming
- AGCM SST Patch Experiments

Key Points:

- Reversal in ISM–Equatorial Indian Ocean SST Relationship post-2000 period
- High-resolution AGCM SST patch experiments isolate regional SSTA impacts on ISM anomalies
- Accelerated equatorial Indian Ocean warming suppresses ISM through increased local convection, lower-tropospheric heating, and moisture convergence

Abstract

Indian Summer Monsoon (ISM) rainfall exhibits strong sensitivity to sea surface temperature anomalies (SSTAs) across four Indo-Pacific nodal regions: The Western and Eastern Equatorial Indian Ocean (WEIO and EEIO), the Western Pacific (WPAC), and the Niño3.4 region. Historically, positive ISM rainfall anomalies are associated with warming in WEIO and WPAC, while warming in EEIO and Niño3.4 suppresses rainfall. However, observations after 2000 reveal a marked weakening/reversal, of the ISM response to equatorial Indian Ocean SSTAs, whereas its sensitivity to WPAC and Niño3.4 remains largely unchanged. Using high-resolution Atmospheric General Circulation Model (AGCM) SST patch experiments with idealized perturbations, we isolate the influence of these regions on monsoon variability. The simulations indicate that positive SSTAs in the equatorial Indian Ocean enhance local deep convection, lower-tropospheric diabatic heating, and moisture convergence, redistributing convection away from India and weakening ISM rainfall. These findings have important implications for monsoon predictability under a warming climate.

1. Introduction

India, home to over a billion people, receives more than 75% of its annual rainfall during the boreal summer monsoon season (June–September, JJAS). Although the Indian summer monsoon (ISM) is a robust and recurring feature of the annual cycle, the all-India summer monsoon rainfall (ISMR) exhibits significant interannual variability (IAV), with a standard deviation of approximately 10% relative to the climatological mean. This variability has profound impacts on agriculture, water resources, and the broader economy. Therefore, understanding and predicting changes in ISMR is critical for ensuring the region's socio-economic and environmental stability.

ISM is governed by complex land–atmosphere–ocean processes, influenced by both local feedbacks such as monsoon intraseasonal oscillations and remote drivers associated with interannual climate variability. Two dominant modes which modulate ISMR are the El Niño-Southern Oscillation (ENSO; Rasmusson & Carpenter, 1983) over the equatorial Pacific Ocean, and the Equatorial Indian Ocean Oscillation (EQUINOO; Gadgil et al., 2004). ENSO and EQUINOO individually explain approximately 30% and 19% of ISMR variance, respectively (Surendran et al., 2015). In addition to Pacific drivers and SSTAs, convective variability over the equatorial Indian Ocean also exert substantial influence on monsoonal variability via

dynamic competition between the oceanic and continental Tropical Convergence Zone (TCZ) (Sikka & Gadgil, 1980).

Changes in ISMR due to global warming, have been extensively studied (Rajendran et al., 2012, 2013; and references therein). These changes have been attributed to a range of factors including the Indian Ocean warming and reduced land-ocean thermal contrast (Roxy et al., 2015), land use changes (Paul et al., 2018), and aerosol loading (Bollasina et al., 2011; Sajani et al., 2012; Surendran et al., 2022) However, the relative importance of warming of equatorial SST quadrupole (WEIO: 50°–70°E, 10°S–10°N, EEIO: 90°–110°E, 10°S–0°, WPAC: 90°–110°E, 10°S–0° and Niño3.4; 120°–150°E, 5°S–5°N) of ENSO and IOD, for ISMR remains underexplored, particularly the impact of SST warming over the WEIO and EEIO. Given the established influence of equatorial Indian Ocean convection on ISMR, it is important to assess whether the relationship between ISMR and SST quadrupole has remained stable or undergone a shift in recent decades.

A comprehensive evaluation of all generations of Atmospheric and Coupled Model Intercomparison Projects' (AMIP and CMIP) models, including their 6th phase participants (AMIP6 and CMIP6), by Kavirajan Rajendran et al., (2022) demonstrated major deficiencies in capturing the strength and the spatial structure of the relationship of ISMR with boreal summer SST quadrupole. In particular most of the models struggled to simulate the dipole-like SST gradient between the WEIO and EEIO. Alarmingly, several models reproduced an ISMR-equatorial Indian Ocean (EIO) SST relationship with the opposite sign to the observed (Kavirajan Rajendran et al., 2022), including the NCEP-CFSv2 seasonal prediction model (K. Rajendran et al., 2021). The most dominant oceanic mode having the strongest influence on ISMR, has shown considerable variation of ENSO-ISMR correlation over the last century (Fig. S2). These results highlight the importance of understanding the evolving linkage between ISM and equatorial SST quadrupole in the context of warming climate, which is critical for improving seasonal forecasts and future climate projections.

In the past, several modelling studies have investigated the influence of tropical and midlatitude SSTAs on global atmosphere–ocean variability. However, the bulk of tropical SST research has been focused on the Pacific Ocean, with relatively few studies examining the atmospheric response to EIO SST anomalies (Chandrasekar & Kitoh, 1998; Shukla, 1975; Soman & Slingo, 1997; Yamazaki, 1988). For example, Shukla, (1975) showed that imposing

cold SST anomalies over the western Arabian Sea suppressed rainfall over India due to reduced evaporation. Yamazaki, (1988) applied a +2°C SST anomaly over the EIO and observed suppressed July–August rainfall over India and Indochina, attributing it to a weakened land–ocean thermal gradient. In contrast, Soman & Slingo, (1997) found no significant effect on monsoon onset from Indian Ocean SST anomalies. These inconsistencies likely stem from the limitations of older models with inadequate representation of monsoon dynamics and climatology.

Given these challenges, it is essential to revisit the ISMR and SST quadrupole relationship, using newer and high-resolution global climate models that better capture ISM and Indo-Pacific SST climatology and their variability. In this study, we employ the MRI-AGCM, known for its fidelity in representing key features of mean monsoon and its variability (K. Rajendran et al., 2013; Varghese et al., 2020)

We examine the sensitivity of ISM to equatorial Indo-Pacific SST anomalies through idealized high-resolution AGCM simulations. These simulations are designed with prescribed SSTA patches superimposed on global climatological SSTs to isolate the atmospheric response to SST perturbations in four nodal regions: WEIO, EEIO, WPAC, and Niño3.4. Thus, our experimental framework focusing these four domains allows for a clean attribution of monsoon sensitivity to specific SST forcing patterns, thereby enabling a mechanistic understanding of ISMR modulation under present and evolving climate conditions.

This paper is structured with Section 2 detailing the AGCM setup, datasets, and methodology employed for the SSTA patch experiments. Section 3 presents the sensitivity analyses and discusses the underlying physical mechanisms linking ISMR to SSTAs in each region. Section 4 provides a summary of the key findings and their implications for monsoon predictability particularly under climate change.

2. Model, Experiments and Datasets

The model employed in this study is the high-resolution Meteorological Research Institute Atmospheric General Circulation Model version 3.2 (MRI-AGCM3.2) (Mizuta et al., 2012) as described by Varghese et al., (2020). The primary configuration uses a triangular truncation at T_L319 corresponding to a linear Gaussian grid of 640 × 320 points, which yields a horizontal resolution of approximately 60 km. The model includes 64 vertical levels, extending from the

surface up to 0.01 hPa. Deep convection is parameterized using the Yoshimura convection scheme (Yoshimura et al., 2015), which incorporates a cloud-top entrainment process and improved moisture sensitivity.

In the control simulation, the model is forced with climatological SSTs and sea ice concentrations derived from HadISST data (Rayner et al., 2003), averaged over 1979–1999, as the boundary condition. These fields are prescribed globally at each ocean grid point. The control simulation is integrated for 21 years, excluding an initial 1-year spin-up period. In addition to the primary configuration, a very high-resolution experiment is conducted at T_L959 with a linear Gaussian grid of 1920 × 960 points, corresponding to a horizontal resolution of approximately 20 km. This experiment follows the same boundary forcing and experimental design as the T_L319 configuration and is integrated for 13 years, again excluding 1 year for spin-up.

Further, it is shown that the model skilfully reproduces the JJAS climatological mean rainfall and lower-tropospheric circulation at both 60-km and 20-km horizontal resolutions (Fig. 1). The 60-km simulation captures the major monsoon rainfall features, including the core monsoon zone, monsoon trough, and Somali Jet, while the 20-km simulation provides modest improvements in representing orographic rainfall over the Western Ghats and north-eastern India. Both resolutions perform comparably in simulating the strength and structure of low-level westerlies over the Arabian Sea and Bay of Bengal. Overall, the close agreement with GPCP rainfall and NCEP reanalysis fields underscores the model's suitability for investigating regional monsoon dynamics and SST teleconnections.

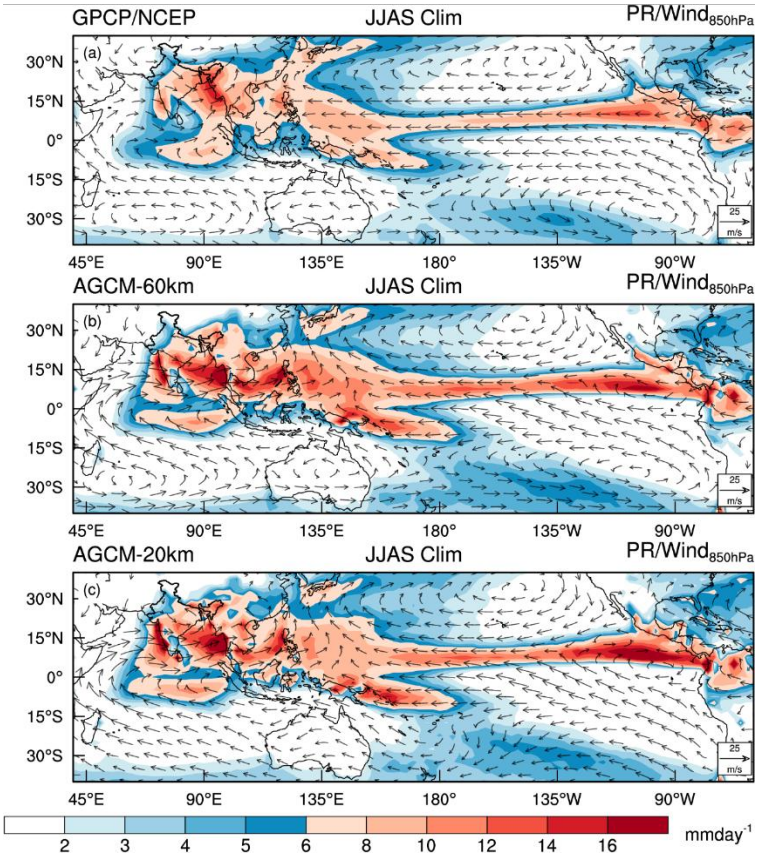

Figure 1: June-September climatological mean rainfall (shaded) and 850 hPa winds (vectors) of (a) GPCP rainfall and NCEP reanalysis winds and MRI-AGCM3.2 at (b) 60-km and (c) 20-km resolution.

2.1. AGCM SST Patch Experiments

A suite of idealized high-resolution AGCM patch experiments were performed to isolate the impact of SSTAs in the four nodal domains (WEIO, EEIO, WPAC and Niño3.4) over the equatorial Indo-Pacific on the ISM. The observed SSTAs during extreme monsoon years in the equatorial Indian Ocean are relatively moderate in magnitude and exhibit greater zonal than meridional extent particularly over EEIO and Niño3.4 (Joseph et al., 1994). To reflect these characteristics, each experiment imposes a moderate but persistent SSTAs (maximum amplitude of ±1°C) superimposed on annually varying climatological SSTs in a specified region, while SSTs outside this domain remain unchanged. The imposed anomalies have a Gaussian horizontal structure with smooth gradients and e-folding decay in both the zonal and meridional directions, ensuring realistic transitions and minimal boundary discontinuities (Fig. 2). For each region, two experiments are conducted, one with a +1°C warming anomaly and another with a −1°C cooling, to assess the linearity and robustness of the atmospheric response.

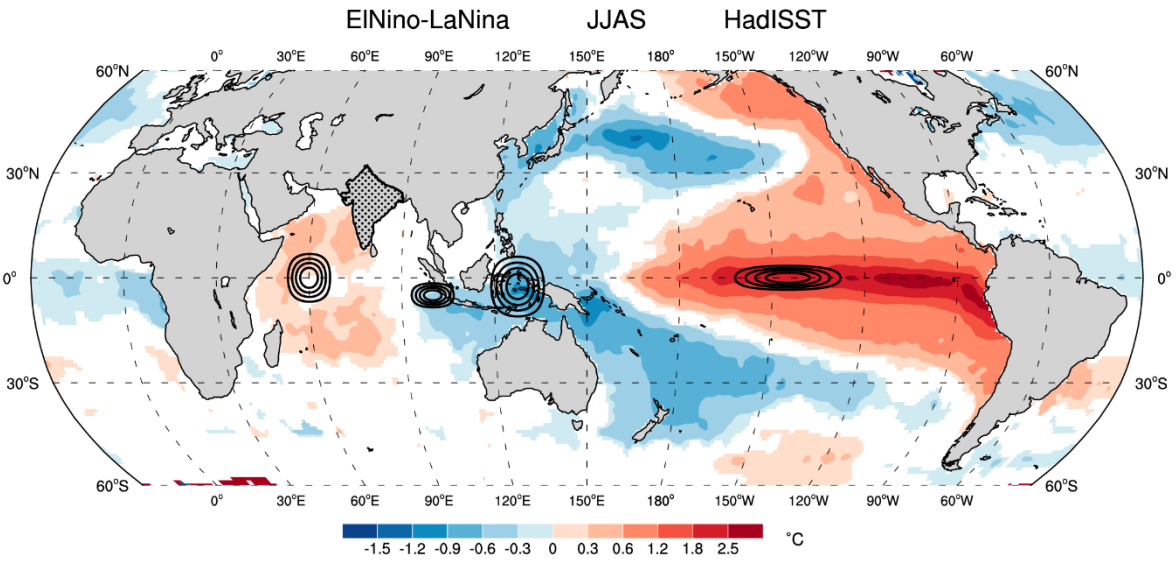

154

155 **Figure 2**. Spatial distribution of the composite sea surface temperature (SST) difference between El
156 Niño and La Niña events. Areas with differences statistically significant at the 95% confidence level
157 are shaded. Also shown is the horizontal structure of the imposed sea surface temperature
158 anomalies (SSTAs) used in the AGCM patch experiments. These correspond to positive SSTA patches
159 (maximum amplitude of +1°C) centred over the Western Equatorial Indian Ocean (WEIO), Eastern
160 Equatorial Indian Ocean (EEIO), Western Pacific (WPAC), and Niño3.4 region. Experiments with
161 negative SSTAs (−1°C; not shown) use the same spatial pattern with reversed sign. SSTs outside the
162 specified patch domains are held at climatological values. The black stippled region shows the MR
163 region.

164 Some experiments are designed to isolate the individual effects of SSTAs in each region, while
165 others explore the combined influence of multiple domains (e.g., WEIO & EEIO in opposite
166 phases for IOD-like forcing, Niño3.4 & WPAC in opposite phases for ENSO-like forcing, and a
167 combination of IOD & ENSO forcing in opposite phases). Thus, in addition to the control run
168 using climatological SSTs over global oceans, sixteen additional SSTA patch experiments were
169 conducted at 60 km resolution, each integrated for 6 years after a 1-year spin-up. A subset of
170 these experiments, totalling four, was also repeated at 20 km resolution, with a 3-year
171 integration after spin-up. The configurations for 22 experiments are summarized in Table 1.

172 **Table 1.** Summary of AGCM SST patch experiments.
173

No.	Experiment Name	Domain, Maximum and Sign of SSTA	Duration	Resolution
1	**CNTL**	Climatological SSTs globally	21 Years	T$_L$319L64 (~60 km)
2	**WEIO-P**	1°C warm SSTA over WEIO	6 Years	″
3	**WEIO-N**	1°C cold SSTA over WEIO	6 Years	″
4	**EEIO-P**	1°C warm SSTA over EEIO	6 Years	″
5	**EEIO-N**	1°C cold SSTA over EEIO	6 Years	″
6	**WPAC-P**	1°C warm SSTA over WPAC	6 Years	″
7	**WPAC-N**	1°C cold SSTA over WPAC	6 Years	″
8	**Niño3.4-P**	1°C warm SSTA over Niño3.4	6 Years	″

9	**Niño3.4-N**	1°C cold SSTA over Niño3.4	6 Years	‘’
10	**IOD-P** *(WEIO-P & EEIO-N)*	1°C warm SSTA over WEIO and 1°C cold SSTA over EEIO	6 Years	‘’
11	**IOD-N** *(WEIO-N & EEIO-P)*	1°C cold SSTA over WEIO and 1°C warm SSTA over EEIO	6 Years	‘’
12	**LaNiña** *(WPAC-P & Niño3.4-N)*	1°C warm SSTA over WPAC and 1°C cold SSTA over Niño3.4	6 Years	‘’
13	**ElNiño** *(WPAC-N & Niño3.4-P)*	1°C cold SSTA over WPAC and 1°C warm SSTA over Niño3.4	6 Years	‘’
14	**IOD-P&ElNiño** *(WEIO-P, EEIO-N, WPAC-N & Niño3.4-P)*	1°C warm SSTA over WEIO, 1°C cold SSTA over EEIO, 1°C cold SSTA over WPAC and 1°C warm SSTA over Niño3.4	6 Years	‘’
15	**IOD-P&LaNiña** *(WEIO-P, EEIO-N, WPAC-P & Niño3.4-N)*	1°C warm SSTA over WEIO, 1°C cold SSTA over EEIO, 1°C warm SSTA over WPAC and 1°C cold SSTA over Niño3.4	6 Years	‘’
16	**IOD-N&ElNiño** *(WEIO-N, EEIO-P, WPAC-N & Niño3.4-P)*	1°C cold SSTA over WEIO, 1°C warm SSTA over EEIO, 1°C cold SSTA over WPAC and 1°C warm SSTA over Niño3.4	6 Years	‘’
17	**IOD-N&LaNiña** *(WEIO-N, EEIO-P, WPAC-P & Niño3.4-N)*	1°C cold SSTA over WEIO, 1°C warm SSTA over EEIO, 1°C warm SSTA over WPAC and 1°C cold SSTA over Niño3.4	6 Years	‘’
18	**CNTL_S** *(Similar to CNTL, but at 20km Super Resolution)*	Climatological SSTs globally	13 Years	T959L64 (~20 km)
19	**IOD-P&ElNiño_S** *(Similar to Exp.14, but at 20km resolution)*	1°C warm SSTA over WEIO, 1°C cold SSTA over EEIO, 1°C cold SSTA over WPAC and 1°C warm SSTA over Niño3.4	3 Years	‘’
20	**IOD-P&LaNiña_S** *(Similar to Exp.15, but at 20km resolution)*	1°C warm SSTA over WEIO, 1°C cold SSTA over EEIO, 1°C warm SSTA over WPAC and 1°C cold SSTA over Niño3.4	3 Years	‘’
21	**IOD-N&ElNiño_S** *(Similar to Exp.16, but at 20km resolution)*	1°C cold SSTA over WEIO, 1°C warm SSTA over EEIO, 1°C cold SSTA over WPAC and 1°C warm SSTA over Niño3.4	3 Years	‘’
22	**IOD-N&LaNiña_S** *(Similar to Exp.17, but at 20km resolution)*	SSTA over WEIO, 1°C warm SSTA over EEIO, 1°C warm SSTA over WPAC and 1°C cold SSTA over Niño3.4	3 Years	‘’

2.2. Observational datasets

To analyse recent climate variability and validate the AGCM simulations, we utilize the following observational and reanalysis datasets for the period 1979–2020:

i. Precipitation data are obtained from the Global Precipitation Climatology Project (GPCP) (Adler et al., 2003).

ii. Sea surface temperature (SST) data are sourced from the Hadley Centre Sea Ice and SST dataset (HadISST1) (Rayner et al., 2003).

iii. Winds are taken from the NCEP/NCAR Reanalysis-2 (Kanamitsu et al., 2002).

iv. Monthly Outgoing Longwave Radiation (OLR), Version 2.7 is taken from NOAA Climate Data Record (CDR) (Hai-Tien Lee and NOAA CDR Program., 2018)

Indian Summer Monsoon Rainfall (ISMR) defined as the June to September (JJAS) mean rainfall averaged over the Indian monsoon region (MR) (Fig. 2) as specified by Gadgil et al., (2019), using the 0.25°×0.25° gridded rainfall dataset developed by Pai et al., (2014) from the India Meteorological Department (IMD).

3. Results

3.1. Shift in the Sensitivity of ISMR to Equatorial Indian Ocean SSTAs

Sensitivity assessment between ISMR and equatorial Indian ocean SSTAs is carried out using correlation maps between outgoing longwave radiation (OLR multiplied by -1.0) as a proxy for convection and regional mean SST over the four nodal Indo-Pacific domains (WEIO, EEIO, WPAC, Niño3.4) during the summer monsoon season (JJAS) for two distinct periods: 1979–2000 and 2001–2020 (Fig. 3). A striking feature is the emergence of a regime shift in ISMR sensitivity to SSTAs over the equatorial Indian Ocean. During 1979–2000, SSTs in the WEIO exhibit weakly positive or near-zero correlations with ISMR, particularly over Central India (Fig. 3a), in contrast to the historically strong positive correlation documented by (Francis & Gadgil, 2010). However, in the post-2000 period, this relationship weakens: warmer SSTs over WEIO are now negatively correlated with convection and rainfall across northern and north-eastern India (Fig. 3e). A clearer sign reversal is evident in the EEIO-ISMR relationship (Figs. 3b and 3f), indicating a fundamental shift in the ISM response to SSTAs in the equatorial Indian Ocean.

More importantly, the coupling between the EIO SST dipole and local convection has strengthened during 2001–2020. This is evident from the enhanced anti-correlation between WEIO and EEIO indices in recent decades. The dipole-like interplay between the two regions has intensified whereby enhanced convection over one lobe is now more closely associated with suppressed convection over the other. This evolution indicates that both WEIO and EEIO have emerged as more active centres of convection under sustained warming, exerting stronger and more direct control on local atmospheric dynamics.

3.2 Persistent Teleconnection with Tropical Pacific SSTAs

In contrast to the evolving ISM-Indian Ocean relationship, the teleconnection between the monsoon and Pacific SSTAs remains largely unchanged across both periods. Warm (cold) anomalies over the Western Pacific (WPAC) continue to enhance (suppress) ISMR or monsoon convection by reinforcing the continental convective maximum (Figs. 3c and 3g). Similarly, warming in the Niño3.4 region remains associated with suppressed ISM convection and reduced ISMR, likely due to subsidence over the Indian region induced by changes in the Walker circulation (Figs. 3d and 3h).

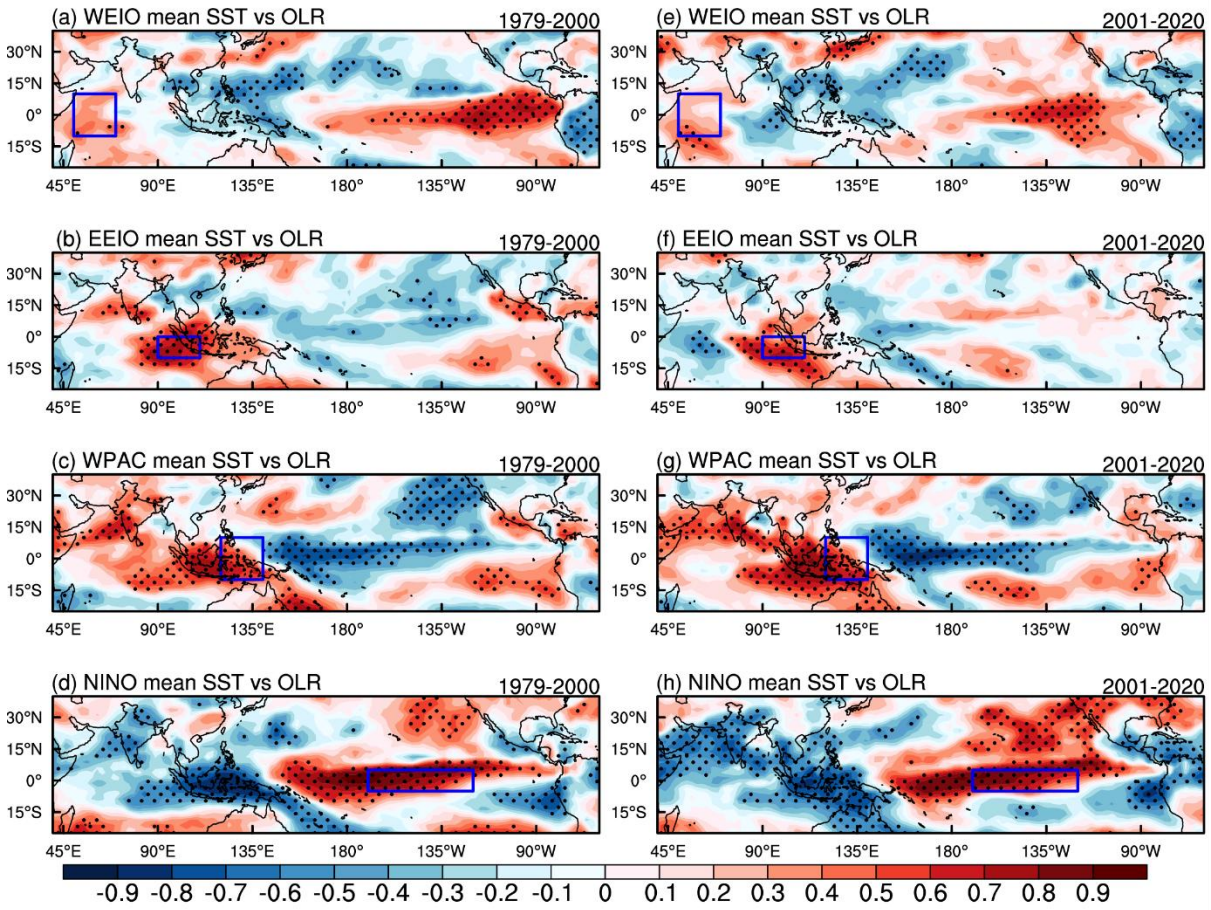

Figure 3. Correlation maps of OLR (×-1.0) with regionally averaged SST over (a, e) WEIO, (b, f) EEIO, (c, g) WPAC, and (d, h) Niño3.4 region (indicated by blue boxes) during the June–September (JJAS) summer monsoon season for two periods: 1979–2000 (left panels: a-d) and 2001–2020 (right panels: e-h) for WEIO, EEIO, WPAC, and Niño3.4 versus OLR for the periods 1979–2000 (panels a–d) and 2001–2020 (panels e–h). Areas with correlations significant at the 95% confidence level are stippled.

These findings emphasize that the Pacific teleconnections, particularly those associated with ENSO, retain their canonical influence on the ISM with minor modulations. Figure 4 further supports this continuity, showing that despite decadal variability, ENSO remains a dominant

driver of ISMR anomalies. In contrast, the equatorial Indian Ocean is undergoing a notable and potentially climate change-driven transformation in its coupling with the ISM.

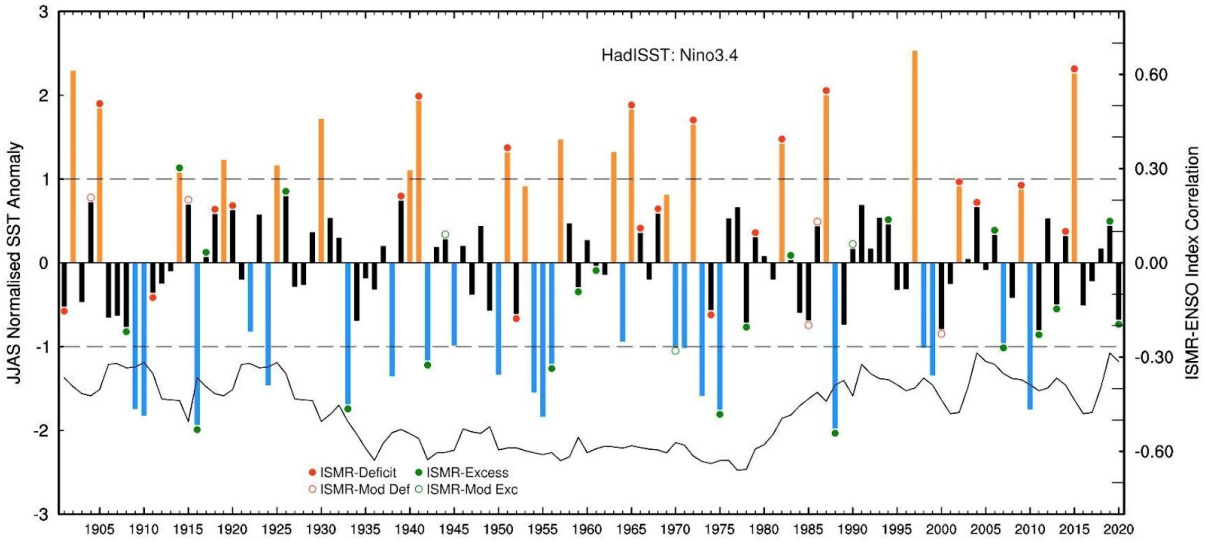

Figure 4. Variation of the normalized ENSO index (Niño3.4 SST anomalies relative to the 31-year moving average) during the June-September (JJAS) season during 1901–2020. El Niño events (shaded in orange) are defined as the seasons with anomalies greater than +0.8 and La Niña events (shaded in blue) as those with anomalies less than –0.8. Indian Summer Monsoon Rainfall (ISMR averaged over monsoon region (MR) shown in figure S2) anomalies computed as normalised rainfall anomalies relative to 31-year moving average, are highlighted as deficits (<–1), moderate deficits (-0.8 to –0.1), moderate excesses (+0.8 to +1), and excesses (>+1). The 31-year moving correlation between ISMR and ENSO Index is shown as the line curve.

3.3 Accelerated Warming over WEIO

To further investigate the shifting ISM teleconnection with Indian Ocean SSTs, we examined the temporal evolution of SSTs over the WEIO and EEIO regions. The results reveal a pronounced and accelerated warming trend over the WEIO, with a recent rate of 0.188°C per decade, higher than in the earlier period (Fig. 5). In contrast, the EEIO, while also warming, exhibits a notably lower rate of increase in recent decades. This growing asymmetry in warming trend between WEIO and EEIO underscores the weakening of the zonal SST gradient across EIO, which likely plays a critical role in strengthening the local convection and altering the ISM response. This significant warming over the WEIO region has also been reported by Roxy et al., (2015), who showed an anomalous increase of about 1.2°C during 1912–2012. The results from their study point out the asymmetry in the ENSO teleconnection as one of the reasons, whereby El Niño events induce anomalous warming over the western Indian Ocean while La Niña events fail to produce an equivalent cooling. A second, prominent reason

is the positive SST skewness associated with ENSO, as the frequency of El Niño events has increased during recent decades.

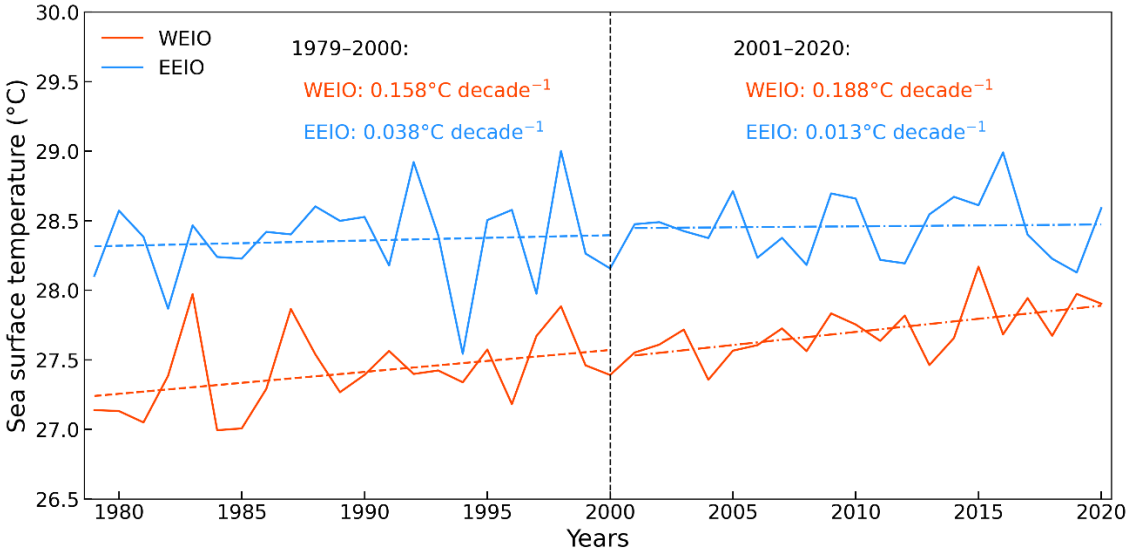

Figure 5. Variation of observed JJAS mean SST (°C) averaged over (a) WEIO and EEIO, as indicated in Figure 3. Trend lines for the periods 1979–2000 and 2001–2020 are shown, with the corresponding rates of increase per decade noted at the top of the panel. The black dashed line shows the demarcation of the two time periods.

3.4 Evidence from AGCM SST Patch Experiments

3.4.1 Role of WEIO and EEIO SSTAs

Further insight into the ISM response to equatorial SSTAs is obtained from AGCM SST patch experiments. Simulations with imposed positive and negative SST anomalies over the WEIO and EEIO (WEIO-P/N and EEIO-P/N) confirm that the recent reversal in ISM sensitivity to equatorial Indian Ocean SSTAs is primarily driven by asymmetric basin-wide warming, particularly the accelerated warming of the WEIO. Experiments with negative anomalies (cooling) over these domains further reinforce the conclusions drawn from the warming experiments. WEIO warming enhances convection over the western equatorial Indian Ocean while suppressing convection over northern regions, including India; conversely, WEIO cooling weakens local oceanic convection and strengthens ISMR, especially along the west coast of India (Figs. 6 and 7). The ISM response to EEIO SST perturbations similarly aligns with the correlations shown in Figure. 3b and 3f. EEIO warming intensifies local convection but exerts only weak or negligible influence on ISMR, reinforcing the conclusion that Indian Ocean warming, most notably over the WEIO, is a key driver of the recent shift in ISMR sensitivity to EIO SSTAs.

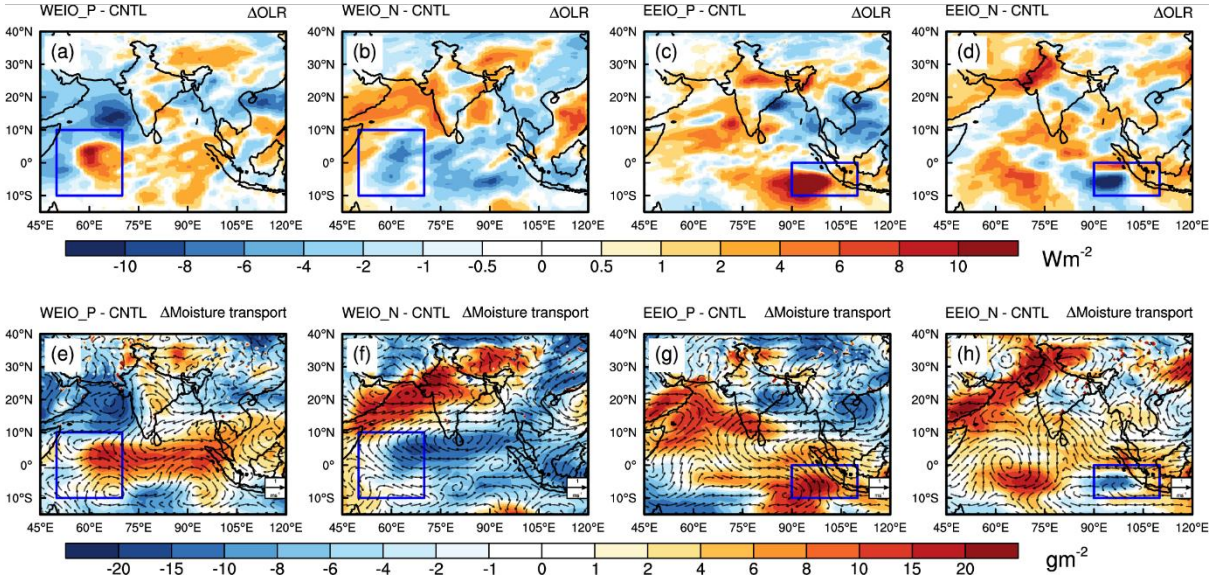

Figure 6: Changes in the June-September mean OLR (×-1.0) (a-d) and changes in mean moisture transport (vectors) and specific humidity (shading) (e-h) from 60km SSTA patch experiments: WEIO-P (WEIO warming), WEIO-N (WEIO cooling, EEIO-P (EEIO warming) and EEIO-N (EEIO cooling) respectively relative to CNTL. WEIO and EEIO are indicated by blue boxes.

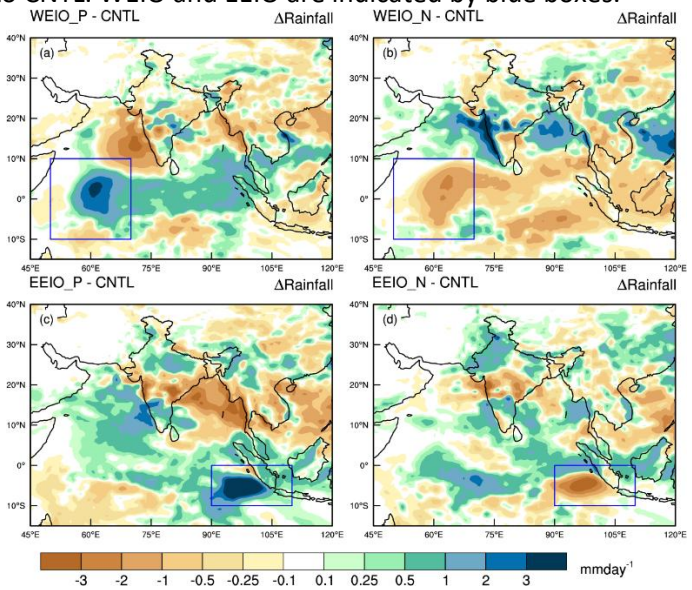

Figure 7: Changes in the June-September mean rainfall from SSTA patch experiments (a) WEIO-P (WEIO warming), (b) WEIO-N (WEIO cooling, (c) EEIO-P (EEIO warming) and (d)EEIO-N (EEIO cooling), relative to the OLR from the 60-km control simulation (CNTL). WEIO and EEIO are indicated by blue boxes.

3.4.2 Local and Remote impacts of SSTAs

The AGCM experiments reveal that EIO SSTAs primarily affect local circulation: warm anomalies enhance vertical motion, convection, and rainfall directly over the perturbed region, while cold anomalies suppress them. The experiments did not show significant or widespread changes in rainfall over the entire Indian subcontinent. But, a significant local effect was observed with a large positive (warm) anomaly in the WEIO, which led to enhanced

moisture transport and specific humidity over the WEIO region, while simultaneously reducing moisture inflow over the west coast of India, thereby weakening ISMR (Fig. 6e-h).

This behaviour aligns with the mechanism proposed by Lindzen & Nigam, (1987), whereby SST-induced temperature gradients generate low-level convergence toward warmer regions, enhancing local evaporation and convection. Such a strengthened equatorial TCZ over the WEIO can inhibit convection over the Indian landmass by altering large-scale vertical motion. Similarly, local convection gets strengthened over EEIO with warm anomalies over there and vice versa.

Consistent with the changes in large-scale circulation, the vertical profiles of convective heating over three representative regions: WEIO, the west coast of India, and central India, exhibit notable anomalies relative to the control simulation, in response to WEIO warming and cooling (Fig. 8). Under WEIO warming, enhanced lower-tropospheric heating and convection are observed over the western Indian Ocean, while heating and rainfall over the Indian subcontinent are suppressed. In contrast, WEIO cooling strengthens tropospheric heating over India and diminishes it over the WEIO, reinforcing the notion of a competitive interaction between oceanic and continental convection zones in the western Indian Ocean basin. These heating anomalies (climatological mean for these experiments are shown in Fig. 9) offer thermodynamic insights into the altered atmospheric response and rainfall redistribution under SST perturbation.

Historically, such competitive behaviour between oceanic and continental TCZs was primarily associated with the warmer eastern and central Indian Ocean (Francis & Gadgil, 2010). However, with the recent acceleration of warming over the WEIO, similar dynamics have now emerged in the western part of the basin as well.

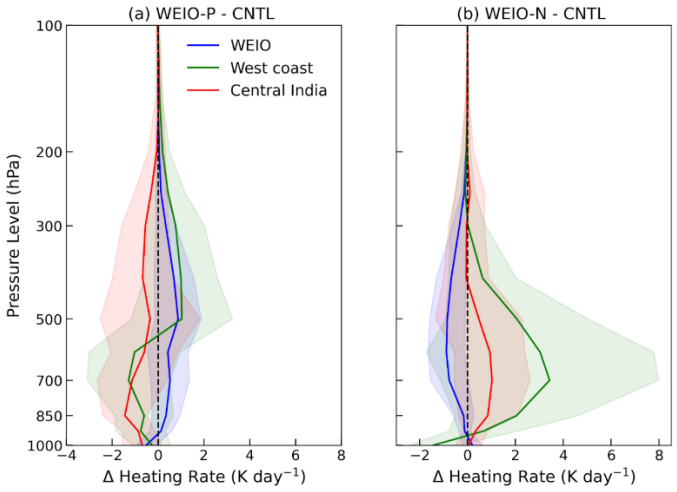

314

315 **Figure 8:** Changes in June-September mean convective heating profile with respect to CNTL, for the
316 two SSTA patch experiments (a) WEIO-P (WEIO warming), and (b) WEIO-N (WEIO cooling) averaged
317 over three regions, WEIO, West Coast of India (8−21.5°N ; 72−77.5°E) and Central India (15.5−25°N ;
318 77.5−88°E). The shaded areas show standard deviation within respective regions.
319

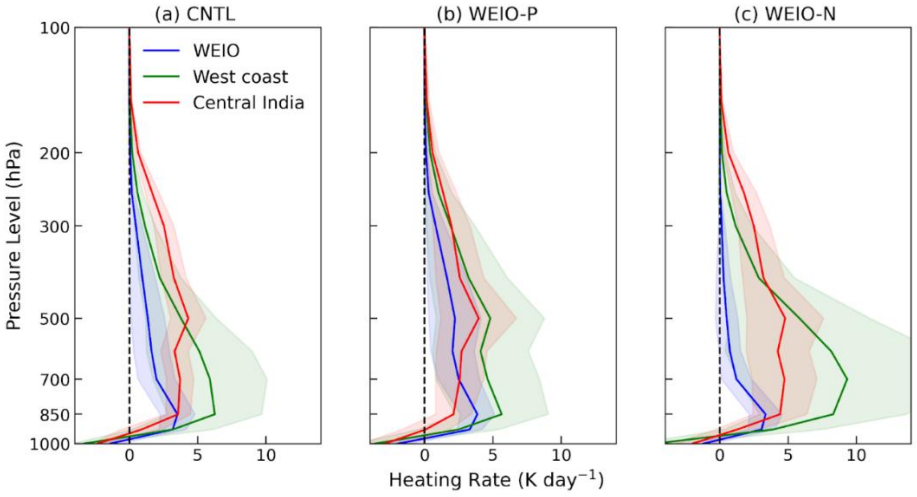

320

321 **Figure 9:** June-September mean convective heating profile from (a) the 60-km control (CNTL) and two
322 SSTA patch experiments (b) WEIO-P (WEIO warming), and (c) WEIO-N (WEIO cooling) averaged over
323 three regions, WEIO, West Coast of India (8−21.5°N ; 72-77.5°E) and Central India (15.5−25°N ; 77.5-
324 88°E).

325 **3.4.4 Dominance of ENSO-ISM relationship**

326 In addition to the correlation-based evidence for a changing ISM–Indian Ocean coupling (Fig.
327 3), the SST-patch sensitivity experiments provide a more direct dynamical assessment of how
328 regional SST forcing modulate large-scale convection, especially that over WEIO. Figure 10
329 illustrates the JJAS mean response of OLR (× –1.0) over the monsoon region (MR) to imposed
330 SST perturbations in the WEIO, EEIO, WPAC, and Niño3.4 domains for the experiments listed
331 in Table 1, at both 60-km and 20-km model resolutions. Consistent with the observed regime

shift, warm SST anomalies over the WEIO induce a weakened convective signal over the Indian monsoon region, whereas cooling produces the opposite response. Notably, the WEIO-forced experiments yield clear and opposing convection anomalies. In contrast, Pacific SST-patch experiments continue to produce robust and statistically significant responses that mirror the strong ENSO teleconnection. The shaded grey intervals in the figure highlight cases where the imposed forcing fails to produce a significant atmospheric response, underscoring the asymmetry and nonlinearity of ISM sensitivity to regional SST anomalies.

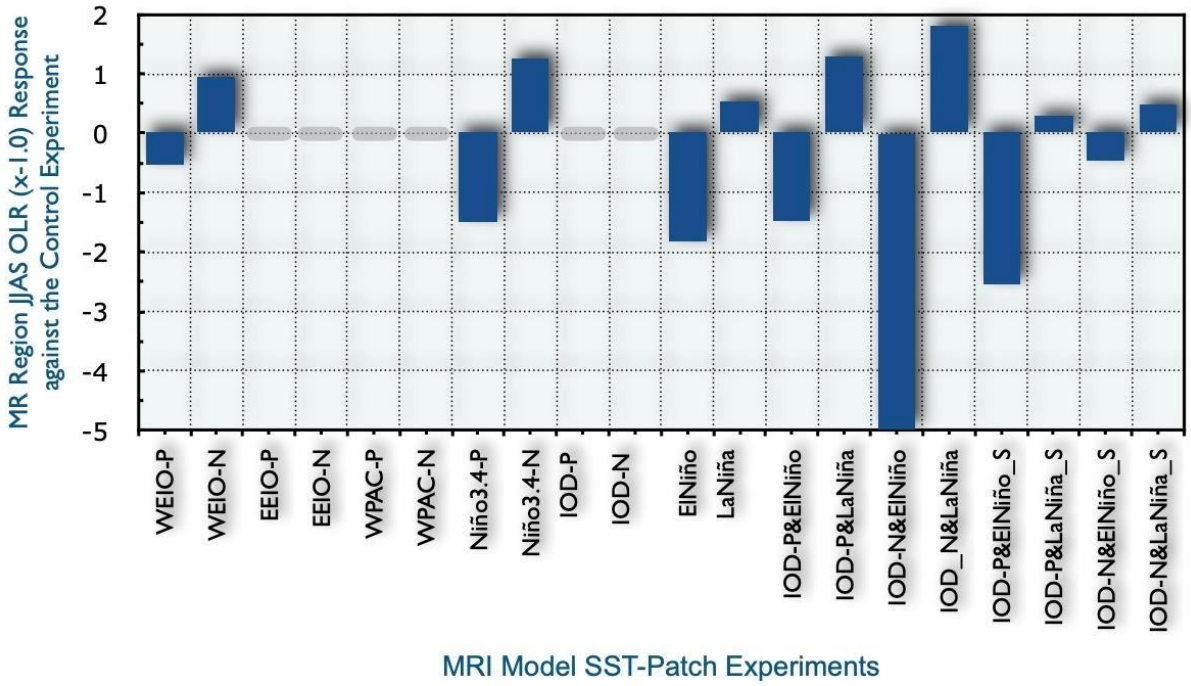

Figure 10: June–September mean Outgoing Longwave Radiation (OLR × –1.0) changes averaged over the Indian monsoon region (MR) for different SST-patch experiments, shown relative to their respective control simulations at 60-km and 20-km resolutions. The grey shaded horizontal boxes indicate experiments that exhibit an insignificant averaged response to the imposed opposing SST forcing.

4. Concluding Remarks

This study investigates the evolving relationship between ISMR and SSTAs in four Indo-Pacific nodal regions: The Western and Eastern Equatorial Indian Ocean (WEIO and EEIO), the Western Pacific (WPAC), and the Niño3.4 region. Using a suite of high-resolution AGCM SST patch experiments with idealized SST perturbations, we systematically assess the relative and combined impacts of these regions on monsoon variability.

Observations highlight a striking regime shift in the ISMR–Indian Ocean SSTA teleconnection in the post-2000 period. While the pre-2000 relationship aligns with the canonical

understanding wherein warming in WEIO and WPAC enhances ISMR and warming in EEIO and Niño3.4 suppresses it, after 2000, this teleconnection has substantially weakened and reversed over the EIO. Despite persistent and accelerated warming in both the WEIO and EEIO, their SSTAs now exhibit little to no statistically robust relationship with ISMR, diverging from their earlier weak positive (WEIO) and negative (EEIO) associations with monsoon variability. This transition appears to be dynamically mediated by enhanced local deep convection, increased lower-tropospheric diabatic heating, and strengthened moisture convergence over the equatorial Indian Ocean under positive SSTA, which appear to redistribute convective activity away from the Indian subcontinent.

In contrast, the ISMR response to SSTAs in the WPAC and Niño3.4 regions remain largely consistent with the historical ISMR-ENSO relationship. The model faithfully captures these canonical teleconnections, lending further confidence to the robustness of the model and the physical mechanisms underlying the observed reversal in the equatorial Indian Ocean's influence.

These findings point to the emergence of a climate change-induced reorganization in Indo-Pacific Ocean-atmosphere coupling and remote impact on ISMR. Notably, faster warming of the WEIO relative to adjacent regions appears to play a dominant role in altering the monsoon's sensitivity to WEIO SSTAs. This emerging pattern has critical implications for monsoon predictability, seasonal forecasting skill, and long-term projections of monsoon rainfall under global warming scenarios.

Going forward, it is essential that climate models capture the evolving SST gradients across the equatorial Indian Ocean and their teleconnections with the Indian monsoon. Improved simulation of these mechanisms in coupled climate models will enhance both operational monsoon forecasts and future climate risk assessments. Additionally, further investigation into the nonlinear interactions between ENSO and IOD/EQUINOO, and background ocean warming will be vital to fully understand the drivers of this regime shift.

While the findings offer important insights into the ISMR response to Indo-Pacific SST anomalies, the limitations also should be noted. First, the AGCM used prescribes SST as a boundary condition and does not simulate a fully coupled ocean–atmosphere system. This restricts the ability to capture air-sea feedbacks, which are particularly strong in the equatorial Indian Ocean. The experimental design also does not account for initial state or

boundary state perturbation effects. To mitigate this, we conducted both positive and negative SSTA experiments, providing a more robust assessment of monsoonal sensitivity.

Moreover, while our results highlight the significant role of EIO SSTAs, we do not suggest that they are the sole drivers of ISMR variability. Other key regions, such as the Bay of Bengal, as well as additional dynamical and thermodynamical factors, also play important roles in shaping the Indian summer monsoon behaviour.

Acknowledgment: The authors gratefully acknowledge insightful discussions with Prof. J. Srinivasan and the late Prof. Sulochana Gadgil.

Data availability:

The monthly precipitation data are obtained from the Global Precipitation Climatology Project (GPCP) (https://psl.noaa.gov/data/gridded/data.gpcp.html). Sea surface temperature (SST) data are sourced from the Hadley Centre Sea Ice and SST dataset (HadISST1) (https://www.metoffice.gov.uk/hadobs/hadisst/data/download.html). Winds are taken from the NCEP/NCAR Reanalysis-2(https://psl.noaa.gov/data/gridded/data.ncep.reanalysis2.html). Monthly Outgoing Longwave Radiation (OLR), Version 2.7 is taken from NOAA Climate Data Record (CDR) (https://www.ncei.noaa.gov/metadata/geoportal/rest/metadata/item/gov.noaa.ncdc:C01561/html). The model simulation data used in this study are available from the corresponding author upon reasonable request.

References:

Adler, R. F., Huffman, G. J., Chang, A., Ferraro, R., Xie, P. P., Janowiak, J., et al. (2003). The version-2 global precipitation climatology project (GPCP) monthly precipitation analysis (1979-present). *Journal of Hydrometeorology*, *4*(6), 1147–1167. https://doi.org/10.1175/1525-7541(2003)004<1147:TVGPCP>2.0.CO;2

Bollasina, M. A., Ming, Y., & Ramaswamy, V. (2011). Anthropogenic aerosols and the weakening of the south asian summer monsoon. *Science*, *334*(6055), 502–505. https://doi.org/10.1126/science.1204994

Chandrasekar, A., & Kitoh, A. (1998). Impact of localized sea surface temperature anomalies over the equatorial Indian Ocean on the Indian summer monsoon. *Journal of the Meteorological Society*

414 *of Japan*, *76*(6), 841–853. https://doi.org/10.2151/jmsj1965.76.6_841

415 Francis, P. A., & Gadgil, S. (2010). Towards understanding the unusual indian monsoon in 2009.
416 *Journal of Earth System Science*, *119*(4), 397–415. https://doi.org/10.1007/s12040-010-0033-6

417 Gadgil, S., Vinayachandran, P. N., Francis, P. A., & Gadgil, S. (2004). Extremes of the Indian summer
418 monsoon rainfall, ENSO and equatorial Indian Ocean oscillation. *Geophysical Research Letters*,
419 *31*(12), 2–5. https://doi.org/10.1029/2004GL019733

420 Gadgil, S., Rajendran, K., & Pai, D. S. (2019). A new rain-based index for the Indian summer monsoon
421 rainfall. *Mausam*, *70*(3), 485–500. https://doi.org/10.54302/mausam.v70i3.253

422 Joseph, P. V., Eischeid, J. K., & Pyle, R. J. (1994). Interannual variability of the onset of the Indian
423 summer monsoon and its association with atmospheric features, El Nino, and sea surface
424 temperature anomalies. *Journal of Climate*, *7*(1), 81–105. https://doi.org/10.1175/1520-
425 0442(1994)007<0081:IVOTOO>2.0.CO;2

426 Kanamitsu, M., Ebisuzaki, W., Woollen, J., Yang, S. K., Hnilo, J. J., Fiorino, M., & Potter, G. L. (2002).
427 NCEP-DOE AMIP-II reanalysis (R-2). *Bulletin of the American Meteorological Society*, *83*(11).
428 https://doi.org/10.1175/bams-83-11-1631

429 Lindzen, R. S., & Nigam, S. (1987). On the Role of Sea Surface Temperature Gradients in Forcing Low-
430 Level Winds and Convergence in the Tropics. *Journal of the Atmospheric Sciences*, *44*(17),
431 2418–2436. https://doi.org/10.1175/1520-0469(1987)044<2418:otross>2.0.co;2

432 Mizuta, R., Yoshimura, H., Murakami, H., Matsueda, M., Endo, H., Ose, T., et al. (2012). Climate
433 simulations using MRI-AGCM3.2 with 20-km grid. *Journal of the Meteorological Society of*
434 *Japan*, *90*(A), 233–258. https://doi.org/10.2151/jmsj.2012-A12

435 Pai, D. S., Sridhar, L., Rajeevan, M., Sreejith, O. P., Satbhai, N. S., & Mukhopadhyay, B. (2014).
436 Development of a new high spatial resolution (0.25° × 0.25°) long period (1901-2010) daily
437 gridded rainfall data set over India and its comparison with existing data sets over the region.
438 *Mausam*, *65*(1), 1–18. https://doi.org/10.54302/mausam.v65i1.851

439 Paul, S., Ghosh, S., Mathew, M., Devanand, A., Karmakar, S., & Niyogi, D. (2018). Increased Spatial
440 Variability and Intensification of Extreme Monsoon Rainfall due to Urbanization. *Scientific*
441 *Reports*, *8*(1), 1–10. https://doi.org/10.1038/s41598-018-22322-9

442 Rajendran, K., Kitoh, A., Srinivasan, J., Mizuta, R., & Krishnan, R. (2012). Monsoon circulation
443 interaction with Western Ghats orography under changing climate: Projection by a 20-km mesh
444 AGCM. *Theoretical and Applied Climatology*, *110*(4), 555–571. https://doi.org/10.1007/s00704-
445 012-0690-2

446 Rajendran, K., Sajani, S., Jayasankar, C. B., & Kitoh, A. (2013). How dependent is climate change
447 projection of Indian summer monsoon rainfall and extreme events on model resolution?
448 *Current Science*, *104*(10), 1409–1418.

449 Rajendran, K., Surendran, S., Varghese, S. J., & Chakraborty, A. (2021). Do Seasonal Forecasts of
450 Indian Summer Monsoon Rainfall Show Better Skill with February Initial Conditions? *Current*
451 *Science*, *120*(12), 1863–1874. https://doi.org/10.18520/cs/v120/i12/1863-1874

452 Rajendran, Kavirajan, Surendran, S., Varghese, S. J., & Sathyanath, A. (2022). *Simulation of Indian*
453 *summer monsoon rainfall, interannual variability and teleconnections: evaluation of CMIP6*
454 *models*. *Climate Dynamics* (Vol. 58). Springer Berlin Heidelberg.
455 https://doi.org/10.1007/s00382-021-06027-w

456 Rasmusson, E. M., & Carpenter, T. H. (1983). The relationship between eastern equatorial Pacific sea
457 surface temperatures and rainfall over India and Sri Lanka. *Monthly Weather Review*, *111*(3),
458 517–528. https://doi.org/10.1175/1520-0493(1983)111<0517:TRBEEP>2.0.CO;2

459 Rayner, N. A., Parker, D. E., Horton, E. B., Folland, C. K., Alexander, L. V., Rowell, D. P., et al. (2003).
460 Global analyses of sea surface temperature, sea ice, and night marine air temperature since the
461 late nineteenth century. *Journal of Geophysical Research: Atmospheres*, *108*(14).
462 https://doi.org/10.1029/2002jd002670

463 Roxy, M. K., Ritika, K., Terray, P., Murtugudde, R., Ashok, K., & Goswami, B. N. (2015). Drying of
464 Indian subcontinent by rapid Indian ocean warming and a weakening land-sea thermal
465 gradient. *Nature Communications*, *6*(May). https://doi.org/10.1038/ncomms8423

466 Sajani, S., Krishna Moorthy, K., Rajendran, K., & Nanjundiah, R. S. (2012). Monsoon sensitivity to
467 aerosol direct radiative forcing in the community atmosphere model. *Journal of Earth System*
468 *Science*, *121*(4), 867–889. https://doi.org/10.1007/s12040-012-0198-2

469 Shukla, J. (1975). Effect of Arabian Sea-Surface Temperature Anomaly on Indian Summer Monsoon:
470 a Numerical Experiment With the Gfdl Model. *Journal of the Atmospheric Sciences*, *32*(3), 503–
471 511. https://doi.org/10.1175/1520-0469(1975)032<0503:EOASST>2.0.CO;2

472 Sikka, D. R., & Gadgil, S. (1980). On the maximum cloud zone and the ITCZ over Indian longitudes
473 during the southwest monsoon. *Monthly Weather Review*, *108*(11), 1840–1853.
474 https://doi.org/10.1175/1520-0493(1980)108<1840:OTMCZA>2.0.CO;2

475 Soman, M. K., & Slingo, J. (1997). Sensitivity of the asian summer monsoon to aspects of sea-surface-
476 temperature anomalies in the tropical pacific ocean. *Quarterly Journal of the Royal*
477 *Meteorological Society*, *123*(538), 309–336. https://doi.org/10.1002/qj.49712353804

Surendran, S., Gadgil, S., Francis, P. A., & Rajeevan, M. (2015). Prediction of Indian rainfall during the summer monsoon season on the basis of links with equatorial Pacific and Indian Ocean climate indices. *Environmental Research Letters*, *10*(9). https://doi.org/10.1088/1748-9326/10/9/094004

Surendran, S., Ajay Anand, K. V., Ravindran, S., & Rajendran, K. (2022). Exacerbation of Indian Summer Monsoon Breaks by the Indirect Effect of Regional Dust Aerosols. *Geophysical Research Letters*, *49*(20), 1–11. https://doi.org/10.1029/2022GL101106

Varghese, S. J., Surendran, S., Ajithkumar, B., Rajendran, K., & Kitoh, A. (2020). Future changes in rice yield over Kerala using climate change scenario from high resolution global climate model projection. *Journal of Earth System Science*, *129*(1). https://doi.org/10.1007/s12040-020-01459-0

Yamazaki, K. (1988). Influence of sea surface temperature anomalies over the Indian Ocean and Pacific Ocean on the tropical atmospheric circulation - A Numerical experiment. *Journal of the Meteorological Society of Japan*, *66*(5), 797–806. https://doi.org/10.2151/jmsj1965.66.5_797

Yoshimura, H., Mizuta, R., & Murakami, H. (2015). A spectral cumulus parameterization scheme interpolating between two convective updrafts with semi-lagrangian calculation of transport by compensatory subsidence. *Monthly Weather Review*, *143*(2), 597–621. https://doi.org/10.1175/MWR-D-14-00068.1